

Fluorescent dyes as efficient photosensitizers for near-infrared Nd³⁺ emission

2 PERKIN

Stephen I. Klink,^a Patrick Oude Alink,^a Lennart Grave,^a Frank G. A. Peters,^a Johannes W. Hofstraat,^b Frank Geurts^c and Frank C. J. M. van Veggel^{*a}

^a Laboratory of Supramolecular Chemistry and Technology and MESA⁺ Research Institute, University of Twente, P.O. Box 217, 7500 AE Enschede, The Netherlands.
E-mail: f.c.j.m.vanveggel@ct.utwente.nl; Fax: +31 4894645; Tel: +31 53 4892987

^b Philips Research, Department of Polymers and Organic Chemistry, Prof. Holstlaan 4, 5656 AA, Eindhoven, The Netherlands

^c Akzo Nobel Chemical Research Arnhem, Department CGS, P.O. Box 9300, 6800 SB Arnhem, The Netherlands

Received (in Cambridge, UK) 22nd September 2000, Accepted 2nd January 2001

First published as an Advance Article on the web 5th February 2001

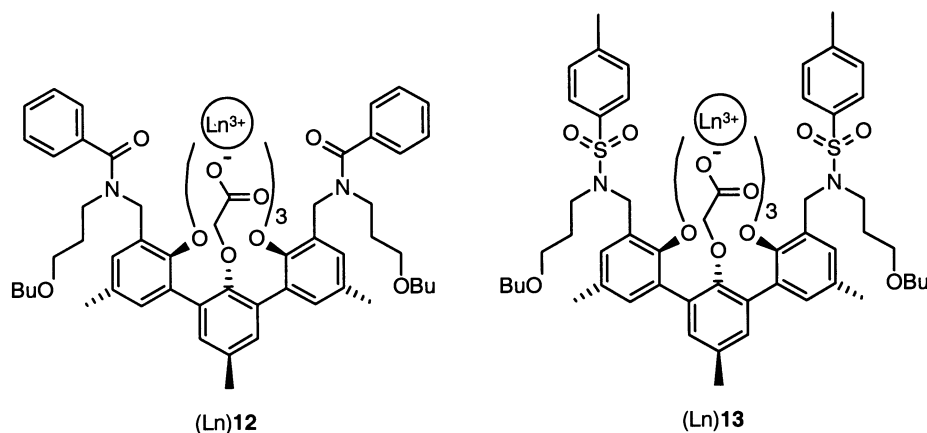
A series of six dye-functionalized Nd³⁺ complexes have been synthesized and their photophysical properties have been studied and evaluated. The incorporated dyes dansyl, coumarine, lissamine, and Texas Red possess broad and intense absorption bands in the visible spectral region and therefore are ideally suitable as photosensitizers for near-infrared Nd³⁺ luminescence, despite their very low intrinsic intersystem crossing quantum yields. The Nd³⁺ complexes display sensitized near-infrared luminescence upon excitation of the dyes. The enhancement of the intersystem crossing quantum yield of the dyes by the complexed Nd³⁺ ions plays a crucial role in the sensitization process.

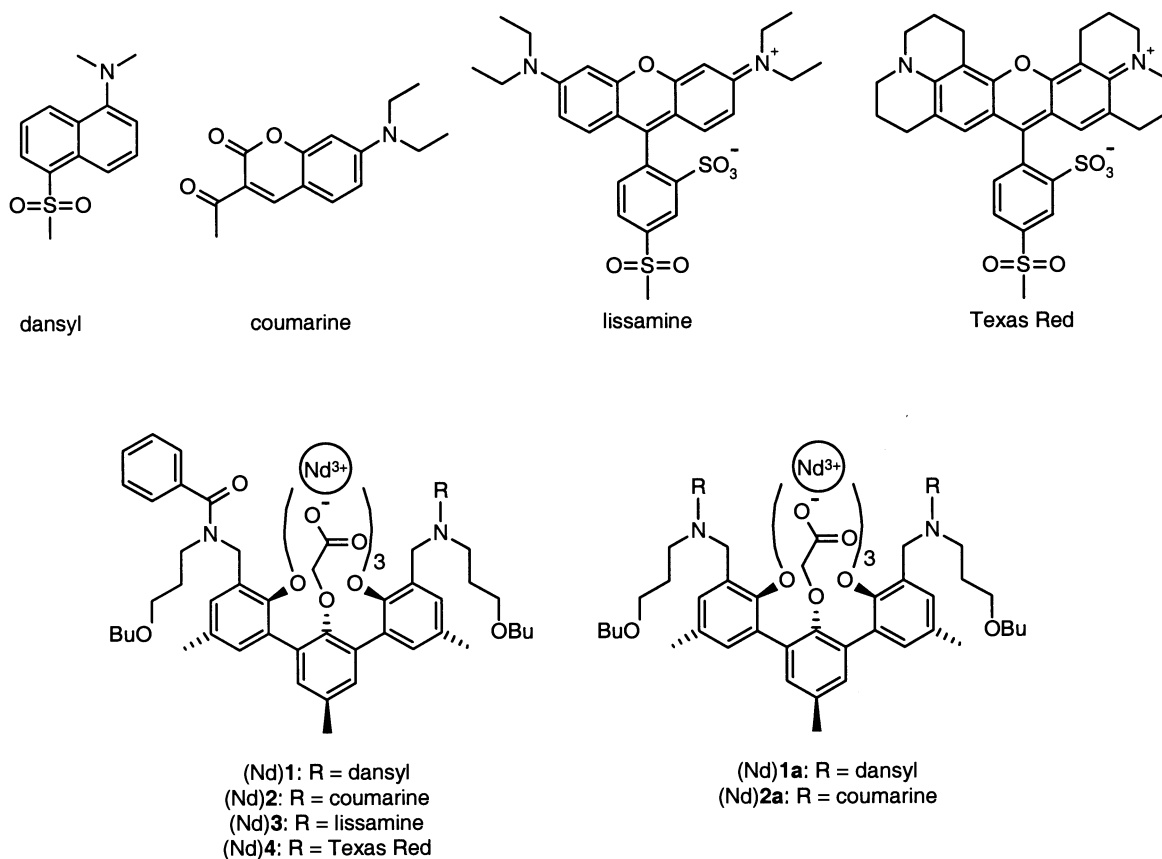
Introduction

Optical signal amplifiers based on lanthanide ions play an important role in optical telecommunication networks, where data are transported as light pulses through silica fibers.¹ With the development of polymers that are transparent in the two standard wavelength regions around 1300 and 1550 nm used for optical data transport,² there has been a growing interest in polymer-based integrated optics.³ For the development of a polymer-based optical amplifier, the lanthanide ions neodymium (Nd³⁺) and erbium (Er³⁺) are ideally suitable as the optically active component, because of their intra-4f transitions at 1330 and 1550 nm, respectively. Since lanthanide ions are in general not very soluble in organic solvents and polymers, the ions have to be encapsulated by an organic ligand in order to improve their processibility. Previously, we have developed a series of *m*-terphenyl-based ligands that form stable and neutral 1:1 complexes with the trivalent lanthanide ions.⁴ In these ligands the lanthanide ion is complexed in a cavity of eight oxygen donor atoms: three bidentate oxyacetate moieties and two amide oxygens or two sulfonamide oxygens.

The corresponding complexes of Nd³⁺, Er³⁺, and Yb³⁺ exhibit near-infrared luminescence in solution. It appeared that their luminescence lifetimes are mainly governed by non-radiative deactivation *via* vibronic coupling of the 4f electronic states and high-energy oscillators in the local (organic) environment.⁴ From this viewpoint, Nd³⁺ is a more attractive candidate than Er³⁺, because of its higher intrinsic luminescence quantum yield in organic environments.^{4,5}

Besides the solubility and stability of the complexes, an efficient population of the lanthanide luminescent state is also required. Direct excitation is very demanding because the optical transitions within the 4f subshells of lanthanide ions are parity forbidden. As a result, the absorption coefficients are very low (typically 1–10 M⁻¹ cm⁻¹) and the lifetimes of the excited states are relatively long (micro- to milliseconds).^{6,7} The indirect excitation by energy transfer from an organic antenna chromophore not only circumvents this excitation problem, but it also allows excitation at wavelengths where the lanthanide ion does not display a significant absorption. For practical applications, the preferable excitation window of the complexes is the visible region, and in particular around 530 or 630 nm. This





would enable the use of green or red diode lasers as excitation sources, which are very compact and available at relatively low costs.

The few reported photosensitizers of Nd^{3+} , Er^{3+} , and Yb^{3+} luminescence that enable visible light excitation are porphyrins,⁸ triphenylmethane derivatives,⁹ and eosin and fluorescein.^{10,11} It is generally accepted that the donating energy level of the antenna is the triplet excited state,¹² which is generated by intersystem crossing from the singlet excited state. Whereas eosin has a modest intersystem crossing yield of 0.33, fluorescein has a very low intersystem crossing yield of 0.02.¹³ However, it was found that the presence of a lanthanide ion significantly reduced the fluorescence intensity of the fluorescein antenna.^{11,14} Also in other antenna-lanthanide systems this effect has been observed.^{5,15} This phenomenon is generally referred to as the *external heavy atom effect*.¹⁶ The presence of the heavy and paramagnetic lanthanide ion increases the spin-forbidden intersystem crossing process of the antenna chromophore at the expense of the antenna fluorescence.

In this article we present the synthesis and a systematic study of *m*-terphenyl-based Nd^{3+} complexes that have been functionalized with fluorescent dyes as photosensitizers for Nd^{3+} luminescence. The efficiency of the sensitization process in the different complexes has been compared, and the intersystem crossing yield of the antenna has been studied by monitoring the antenna fluorescence. The incorporated dyes dansyl, coumarine, lissamine, and Texas Red have intense absorption bands ranging from 350 to 600 nm with triplet states that are high enough in energy to populate the Nd^{3+} $^4\text{F}_{3/2}$ luminescent state, which has an energy of 11400 cm^{-1} (see Fig. 1). Previously, we have developed a synthetic route to mono-functionalize the *m*-terphenyl ligands with an antenna chromophore.⁵

Furthermore, we have synthesized complexes that bear two dansyl or two coumarine antenna chromophores, instead of only one. The photophysical properties of these complexes have been studied in order to investigate whether the incorporation

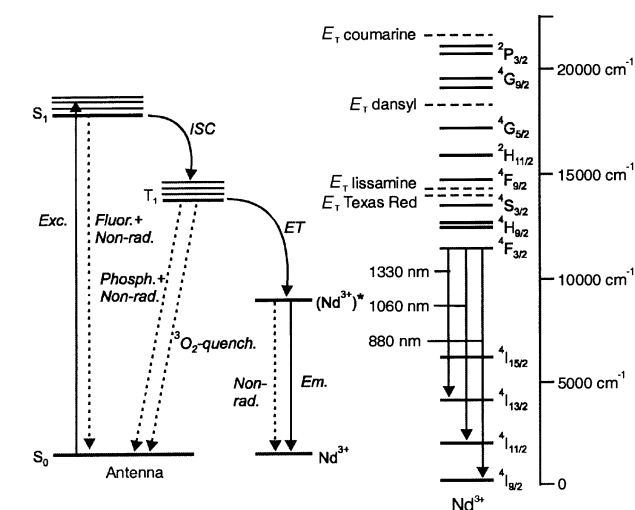


Fig. 1 Photophysical model that describes the sensitization process (left). After excitation of the antenna chromophore into its singlet excited state, intersystem crossing takes place to the triplet state, and subsequently the excitation energy is transferred to the 4f states of the Nd^{3+} ion, ultimately resulting in sensitized Nd^{3+} emission. A detailed scheme of the 4f energy levels of Nd^{3+} as well as the approximate triplet energies of the incorporated dyes is depicted on the right (adapted from G. Stein and E. Würzberg, *J. Chem. Phys.*, 1975, **62**, 20).

of an additional antenna chromophore improves the efficiency of the sensitization process.

Experimental

Synthesis

Melting points were determined with a Reichert melting point apparatus and are uncorrected. Mass spectra were recorded with a Finnigan MAT 90 spectrometer using *m*-NBA (nitrobenzyl alcohol) as a matrix, unless stated otherwise. IR spectra

were obtained using a Perkin Elmer Spectrum BX FT-IR System. ^1H NMR and ^{13}C NMR spectra were recorded with a Bruker AC 250 spectrometer in CDCl_3 using residual solvent peaks as the internal standard, unless stated otherwise. Preparative column chromatography separations were performed on Merck silica gel (particle size 0.040–0.063 mm, 230–400 mesh). Preparative thin layer chromatography was performed on Merck aluminium oxide 150F₂₅₄ plates with a layer thickness of 1.5 mm. CH_2Cl_2 , CHCl_3 , and hexane (mixed isomers) were distilled from CaCl_2 and stored over molecular sieves (4 Å). Ethyl acetate was distilled from K_2CO_3 and stored over molecular sieves (4 Å). Triethylamine (Et_3N) was distilled *in vacuo* and stored over KOH. Acetone and methanol were of analytical grade and were dried over molecular sieves prior to use (4 Å and 3 Å, respectively). Di-*n*-butylamine and dansyl chloride were purchased from Aldrich and used without further purification. Lissamine (sulfonyl chloride mixture of isomers), Texas Red (sulfonyl chloride mixture of isomers), and 7-(diethylamino)coumarin-3-acetic acid were purchased from Molecular Probes and used without further purification. Bis(amine) **5** and mono(amide) **6** have been synthesized according to previously published methods.^{4,5} All reactions were carried out under an argon atmosphere. Standard workup means that the organic layers were finally washed with water, dried over magnesium sulfate (MgSO_4), filtered, and concentrated to dryness *in vacuo*.

Mono(dansyl) triester (7)

To a solution of mono(amide) **6** (0.63 g, 0.59 mmol) and Et_3N (0.22 g, 2.2 mmol) in CH_2Cl_2 (30 mL) was added dansyl chloride (0.18 g, 0.65 mmol). The resulting solution was stirred overnight at rt. The reaction mixture was diluted with CH_2Cl_2 (100 mL) and successively washed with 0.5 M HCl and 0.5 M KOH, followed by standard workup. The crude product was purified by flash column chromatography (ethyl acetate–hexane 45:55 (v/v)) to give **7** as a light-green solid in 51% yield, mp 43–45 °C. δ_{H} 8.54 (d, 1H, *J* 8.5), 8.44 (d, 1H, *J* 8.5), 8.25 (d, 1H, *J* 8.5), 7.63–7.48 (m, 2H), 7.45–7.30 (m, 5H), 7.20 (d, 1H, *J* 8.5), 7.17–6.95 (m, 6H), 5.06–4.71 (m, 4H), 4.18–3.82 (m, 6H), 3.68–3.14 (m, 12H), 2.91 (s, 6H), 2.34 (s, 3H), 2.11 (s, 6H), 2.08–1.71 (m, 4H), 1.60–1.15 (m, 35H), 0.97–0.80 (m, 6H); δ_{C} 172.3, 167.9, 167.1, 136.5–126.6, 125.1, 122.9, 81.5, 80.4, 70.6–67.6, 46.9, 31.8, 27.9, 21.0, 19.2, 14.2; *m/z* (FABMS) 1308.7 [(M + Na)⁺, calc.: 1308.7]. Found: C, 67.5; H, 7.6; N, 3.25; S, 2.1. Calc. for $\text{C}_{74}\text{H}_{99}\text{N}_3\text{O}_{14}\text{S}\cdot 0.5\text{CH}_2\text{Cl}_2$: C, 67.3; H, 7.6; N, 3.26; S, 2.4%.

Bis(dansyl) triester (7a)

To a solution of bis(amine) **5** (1.00 g, 1.00 mmol) and Et_3N (1.32 g, 13.2 mmol) in CH_2Cl_2 (100 mL) was added dansyl chloride (0.63 g, 2.20 mmol). The resulting solution was stirred overnight at rt. The reaction mixture was diluted with CH_2Cl_2 (100 mL) and successively washed with 0.5 M HCl and 0.5 M KOH, followed by standard workup. The crude product was purified by flash column chromatography (gradient from hexane to ethyl acetate–hexane 40:60 (v/v)) to give **7a** as a light-green solid in 80% yield, mp 49–51 °C; δ_{H} 8.51 (d, 2H, *J* 8.5), 8.39 (d, 2H, *J* 8.5), 8.22 (d, 2H, *J* 8.5), 7.60–7.40 (m, 4H), 7.18 (d, 2H, *J* 8.5), 7.04 (s, 2H), 6.97–6.92 (m, 4H), 4.77 (s, 4H), 3.98 (s, 4H), 3.86 (s, 2H), 3.50–3.10 (m, 12H), 2.87 (s, 12H), 2.30 (s, 3H), 2.09 (s, 6H), 1.85–1.55 (m, 8H), 1.40–1.15 (m, 31H), 0.86 (t, 6H, *J* 7.2); δ_{C} 167.5, 166.6, 151.6, 151.2, 150.7, 135.1, 132.8, 132.6–127.4, 122.6, 119.4, 114.6, 81.1, 80.5, 69.9–67.5, 44.9, 44.6, 31.2, 27.6–27.3, 20.1, 18.7, 13.4; *m/z* (FABMS) 1437.1 [(M + Na)⁺, calc. 1437.7]. Found: C, 64.3; H, 7.4; N, 4.0; S, 4.1. Calc. for $\text{C}_{79}\text{H}_{106}\text{N}_4\text{O}_{15}\text{S}_2\cdot\text{CH}_2\text{Cl}_2$: C, 64.0; H, 7.25; N, 3.7; S, 4.3%.

Mono(coumarine) triester (8)

A solution of mono(amide) **6** (0.40 g, 0.38 mmol) and DMAP

(0.11 g, 0.57 mmol) in CH_2Cl_2 (10 mL) was cooled to 0 °C. Subsequently, 7-(diethylamino)coumarin-3-acetic acid (0.100 g, 0.38 mmol) and EDC·HCl (0.11 g, 0.57 mmol) were added to the solution. The reaction mixture was stirred overnight at rt. The reaction mixture was diluted with CH_2Cl_2 (100 mL), and successively washed with 0.5 M HCl and 1 M NaOH, followed by standard workup. The crude product was purified by flash column chromatography (ethyl acetate–hexane 1:1 (v/v)) to give **8** as a green–yellow oil in 47% yield. δ_{H} 7.80–7.62 (m, 1H), 7.53–6.98 (m, 12H), 6.67–6.40 (m, 2H), 5.09–4.71 (m, 4H), 4.22–3.80 (m, 6H), 3.71–3.13 (m, 16H), 2.40–2.20 (m, 9H), 2.09–1.76 (m, 4H), 1.70–1.04 (m, 41H), 0.98–0.67 (m, 6H); δ_{C} 167.9, 159.3, 156.7, 152.0, 151.2, 142.7, 134.0–126.7, 109.3, 107.8, 97.4, 81.3, 81.1, 70.0–6.1, 44.6, 31.7, 28.0–26.0, 20.6, 19.4, 13.8, 12.1; *m/z* (FABMS) 1318.6 [(M + Na)⁺, calc. for $\text{C}_{76}\text{H}_{101}\text{N}_3\text{O}_{15}\text{Na}$: 1318.7].

Bis(coumarine) triester (8a)

A solution of bis(amine) **5** (0.73 g, 0.77 mmol) and DMAP (0.14 g, 1.15 mmol) in CH_2Cl_2 (10 mL) was cooled to 0 °C. Subsequently, 7-(diethylamino)coumarin-3-acetic acid (0.20 g, 0.77 mmol) and EDC·HCl (0.22 g, 1.15 mmol) were added to the solution. The reaction mixture was stirred overnight at rt. The reaction mixture was diluted with CH_2Cl_2 (100 mL) and washed twice with 5% K_2CO_3 , followed by standard workup. The crude product was purified by preparative thin layer chromatography (MeOH– CH_2Cl_2 10:90 (v/v)) to give **8a** as a green–yellow oil in 48% yield. δ_{H} 7.70–7.56 (m, 2H), 7.32–6.90 (m, 8H), 6.55–6.35 (m, 4H), 5.25–4.63 (m, 4H), 4.09–3.70 (m, 6H), 3.50–3.10 (m, 20H), 2.30–2.10 (m, 9H), 1.90–1.70 (m, 4H), 1.50–0.90 (m, 47H), 0.76 (t, 3H, *J* 12.5); δ_{C} 167.2, 159.4, 156.9, 152.0, 151.2, 133.7–128.5, 109.2, 107.9, 97.2, 81.6, 81.0, 70.6–67.5, 44.9, 42.7, 31.5, 31.7, 28.6–27.4, 20.9, 19.4, 14.0, 12.4; *m/z* (FABMS) 1457.7 [(M + Na)⁺, calc. for $\text{C}_{83}\text{H}_{110}\text{N}_4\text{O}_{17}\text{Na}$: 1457.7].

Lissamine triester (9)

To a solution of mono(amide) **6** (0.13 g, 0.12 mmol) and Et_3N (0.05 g, 0.50 mmol) in CH_2Cl_2 (50 mL) was added lissamine-sulfonyl chloride (0.14 g, 0.25 mmol). The resulting solution was stirred overnight at rt. The reaction mixture was diluted with CH_2Cl_2 (100 mL) and successively washed with 1 M HCl, 0.5 M KOH and 1 M HCl, followed by standard workup. The crude product was purified by preparative thin layer chromatography (MeOH– CH_2Cl_2 5:95 (v/v)) to give **9** as a dark-purple solid in 44% yield, mp 171–173 °C. δ_{H} 8.85 (s, 1H), 8.00 (d, 1H, *J* 8.5), 7.43–6.80 (m, 14H), 6.81 (d, 2H, *J* 8.5), 6.69 (s, 2H), 5.10–4.65 (m, 4H), 4.20–3.85 (m, 6H), 3.70–3.20 (m, 20H), 2.25 (s, 9H), 2.05–1.65 (m, 8H), 1.60–1.10 (m, 43H), 0.90–0.70 (m, 6H); δ_{C} 172.3, 168.6, 166.8, 159.0, 157.4, 148.1, 141.3, 133.2–126.1, 113.9, 112.8, 95.1, 81.0, 80.5, 70.3–67.6, 49.2, 46.7, 31.2, 28.6–27.0, 20.4–18.8, 13.4, 12.1; *m/z* (FABMS) 1615.8 [(M + H)⁺, calc. 1615.0]. Found: C, 66.0; H, 7.4; N, 3.8; S, 4.0. Calc. for $\text{C}_{89}\text{H}_{116}\text{N}_4\text{O}_{18}\text{S}_2\cdot\text{H}_2\text{O}$: C, 66.3; H, 7.4; N, 3.5; S, 4.0%.

Texas Red triester (10)

To a solution of mono(amide) **6** (84 mg, 0.08 mmol) and Et_3N (34 mg, 0.32 mmol) in CH_2Cl_2 (25 mL) was added Texas Red sulfonyl chloride (100 mg, 0.16 mmol). The resulting solution was stirred overnight at rt. The reaction mixture was diluted with CH_2Cl_2 (100 mL) and successively washed with 1 M HCl and 1 M KOH, followed by standard workup. The crude product was purified by preparative thin layer chromatography (MeOH– CH_2Cl_2 5:95 (v/v)) to give **10** as a dark-purple solid in 46% yield, mp 126–128 °C. δ_{H} 8.81 (s, 1H), 7.90 (d, 1H, *J* 7.8), 7.45–6.90 (m, 12H), 6.74 (s, 2H), 5.00–4.60 (m, 4H), 4.13–3.80 (m, 6H), 3.60–2.60 (m, 22H), 2.26 (s, 9H), 2.10–1.60 (m, 10H), 1.45–1.10 (m, 43H), 0.90–0.70 (m, 6H); δ_{C} 172.8, 167.5, 155.7,

151.8, 148.9, 140.9, 136.2–122.5, 113.3, 104.0, 81.1, 70.1–67.6, 50.4, 49.9, 46.7–42.6, 31.3, 28.6–26.9, 20.5–18.9, 13.4; *m/z* (FABMS) 1640.5 [(M+Na)⁺, calc. 1640.8]. Found: C, 66.8; H, 7.2; N, 3.4; S, 3.7. Calc. for C₉₃H₁₁₆N₄O₁₈S₂·H₂O: C, 67.3; H, 7.2; N, 3.4; S, 3.9%.

Dibutylsissamine (11)

To a solution of di-*n*-butylamine (56 mg, 0.12 mmol) and Et₃N (45 mg, 0.44 mmol) in CH₂Cl₂ (50 mL) was added lissamine (0.50 g, 0.87 mmol). The resulting solution was stirred overnight at rt. The reaction mixture was diluted with CH₂Cl₂ (100 mL) and washed twice with 0.5 M HCl, followed by standard workup. The crude product was purified by preparative thin layer chromatography (MeOH–CH₂Cl₂ 5:95) to give **11** as a dark-red solid in 40% yield, mp 168–170 °C; δ_H 8.74 (s, 1H), 7.91 (d, 1H, *J* 8.0), 7.26 (d, 2H, *J* 8.0), 7.17 (d, 1H, *J* 8.0), 6.77 (d, 2H, *J* 8.0), 6.66 (s, 2H), 3.60–3.45 (m, 8H), 3.31–3.20 (m, 4H), 1.70–1.50 (m, 4H), 1.40–1.25 (m, 16H), 0.93 (t, 6H, *J* 7.2); δ_C 158.4, 157.3, 155.0, 147.9, 141.2, 132.9, 129.2, 126.6, 113.8, 112.9, 95.5, 48.1, 45.4, 30.7, 19.4, 13.3, 12.1; *m/z* (FABMS) 670.3 [(M + H)⁺, calc. 670.3]. Found: C, 60.5; H, 6.8; N, 6.0; S, 8.9. Calc. for: C₃₅H₄₇N₃O₆S₂·0.33CH₂Cl₂: C, 60.8; H, 6.9; N, 6.0; S, 9.2%.

Typical procedure for the synthesis of the triacids (H₃)1–(H₃)4

A solution of 0.10 mmol of the ligands in TFA (25 mL) was stirred overnight at rt. Subsequently, toluene (10 mL) was added, and the TFA–toluene mixture was azeotropically evaporated. The residue was taken up in CH₂Cl₂ (100 mL) and washed twice with 1 M HCl, followed by standard workup. The triacids were obtained as colored solids in nearly quantitative yield.

Mono(dansyl) triacid ((H₃)1). Light-green solid, mp 83–85 °C; δ_H (CD₃OD) 8.56 (d, 1H, *J* 8.1), 8.33 (d, 1H, *J* 8.1), 8.22 (d, 1H, *J* 7.0), 7.65–7.53 (m, 2H), 7.50–7.33 (m, 5H), 7.29 (d, 1H, *J* 7.0), 7.20–6.71 (m, 6H), 5.0–4.64 (m, 4H), 4.27–3.85 (m, 6H), 3.63–3.07 (m, 12H), 2.88 (s, 6H), 2.36 (s, 6H), 2.06 (s, 3H), 2.00–1.62 (m, 4H), 1.60–1.18 (m, 8H), 0.96–0.80 (m, 6H); *m/z* (FABMS) 1140.5 [(M + Na)⁺, calc. 1140.5]. Found: C, 64.6; H, 6.7; N, 3.7; S, 2.4. Calc. for C₆₂H₇₅N₃O₁₄S·2H₂O: C, 64.5; H, 6.9; N, 3.6; S, 2.8%.

Bis(dansyl) triacid ((H₃)1a). Light-green solid, mp 78–80 °C; δ_H (CD₃OD) 8.46 (d, 2H, *J* 8.5), 8.24 (d, 2H, *J* 8.5), 8.12 (d, 2H, *J* 8.5), 7.60–7.40 (m, 4H), 7.18 (d, 2H, *J* 8.5), 7.05 (s, 2H), 6.90 (s, 2H), 6.70 (s, 2H), 4.63 (s, 4H), 4.05–3.80 (m, 6H), 3.40–3.00 (m, 12H), 2.82 (s, 12H), 2.25 (s, 3H), 1.96 (s, 6H), 1.66–1.62 (m, 4H), 1.40–1.12 (m, 8H), 0.78 (t, 6H, *J* 7.5); *m/z* (FABMS) 1247.6 [(M + H)⁺, calc. 1247.5]. Found: C, 62.4; H, 7.5; N, 4.5; S, 4.7. Calc. for C₆₇H₈₂N₄O₁₅S₂·2H₂O: C, 62.7; H, 6.75; N, 4.4; S, 5.0%.

Mono(coumarine) triacid ((H₃)2). Green–yellow solid, mp 94–96 °C; δ_H (CD₃OD) 7.94–7.75 (m, 1H), 7.50–7.32 (m, 5H), 7.23–6.97 (m, 5H), 6.80–6.67 (m, 2H), 6.60–6.50 (m, 2H), 4.98–4.65 (m, 4H), 4.30–3.87 (m, 6H), 3.65–3.10 (m, 16H), 2.47–2.23 (m, 9H), 2.00–1.70 (m, 4H), 1.63–1.00 (m, 14H), 0.97–0.67 (m, 6H); *m/z* (FABMS) 1150.5 [(M + Na)⁺, calc. 1150.5]. Found: C, 65.3; H, 7.4; N, 3.6. Calc. for C₆₄H₇₇N₃O₁₅·3H₂O: C, 65.0; H, 7.1; N, 3.6%.

Bis(coumarine) triacid ((H₃)2a). Green–yellow solid, mp 118–120 °C; δ_H (CD₃OD) 7.84–7.62 (m, 2H), 7.35–6.90 (m, 8H), 6.70–6.55 (m, 2H), 6.59–6.35 (m, 2H), 4.90–4.60 (m, 4H), 4.10–3.90 (m, 6H), 3.60–3.05 (m, 20H), 2.30–2.10 (m, 9H), 1.90–1.70 (m, 4H), 1.50–0.93 (m, 20H), 0.83 (t, 3H, *J* 8.0), 0.62 (t, 3H, *J* 8.0); *m/z* (FABMS) 1289.4 [(M + Na)⁺, calc. 1289.6]. Found:

C, 63.4; H, 7.4; N, 4.5. Calc. for: C₇₁H₈₆N₄O₁₇·4H₂O: C, 63.7; H, 7.1; N, 4.2%.

Lissamine triacid ((H₃)3). Dark-purple solid, mp 145–147 °C; δ_H (CD₃OD) 8.86 (s, 1H), 8.07 (d, 1H), 7.55–7.35 (m, 5H), 7.30–7.10 (m, 9H), 7.10–6.90 (m, 4H), 4.70 (s, 4H), 4.40–4.00 (m, 6H), 3.80–3.20 (m, 20H), 2.49 (s, 9H), 2.00–1.70 (m, 4H), 1.65–1.45 (m, 4H), 1.45–1.20 (m, 16H), 1.00–0.80 (m, 6H); *m/z* (FABMS) 1447.6 [(M + Na)⁺, calc. 1447.2]. Found: C, 63.2; H, 6.7; N, 3.9; S, 4.0. Calc. for: C₇₇H₉₂N₄S₄O₁₈·2H₂O: C, 63.3; H, 6.6; N, 3.8; S, 4.4%.

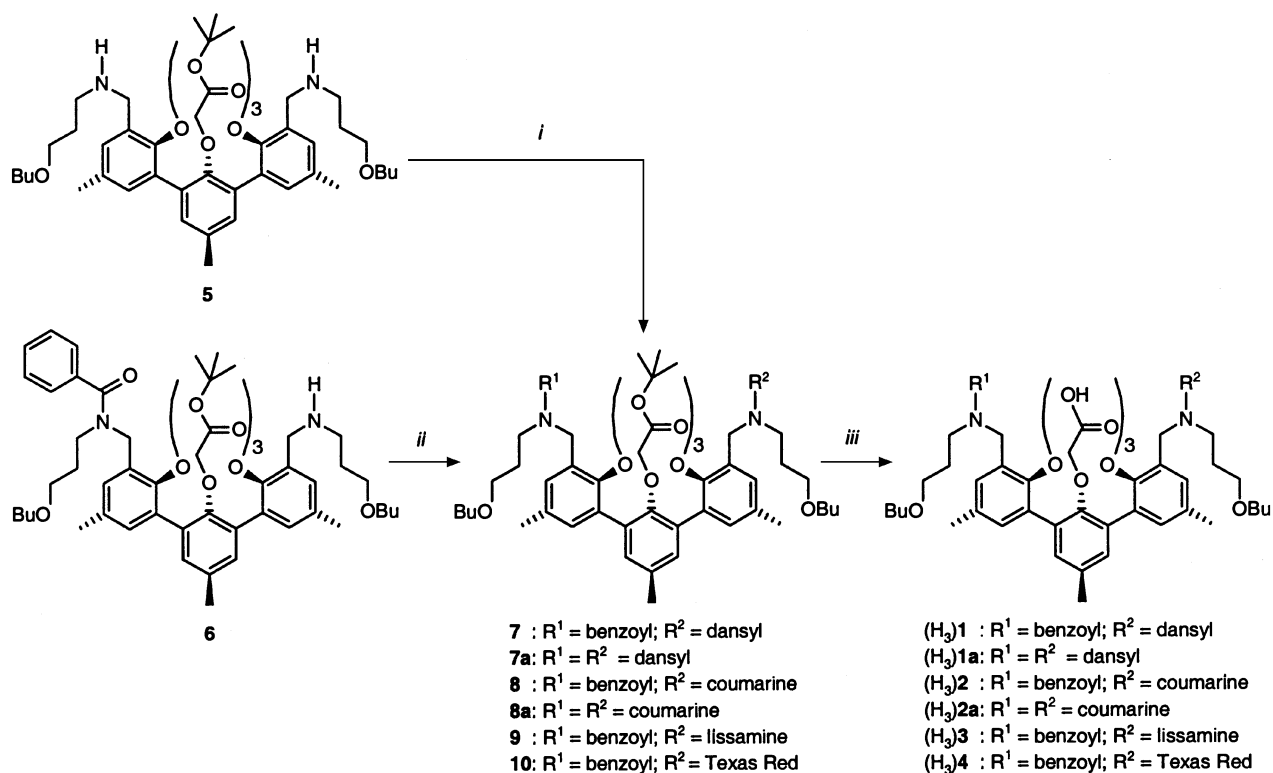
Texas Red triacid ((H₃)4). Dark-purple solid, mp 126–128 °C; δ_H (CD₃OD) 8.80 (s, 1H), 8.01 (d, 1H, *J* 7.8), 7.40–6.87 (m, 12H), 6.57 (s, 2H), 5.00–4.60 (m, 4H), 4.15–3.80 (m, 6H), 3.60–2.60 (m, 22H), 2.26 (s, 9H), 2.10–1.60 (m, 10H), 1.45–1.10 (m, 16H), 0.90–0.70 (m, 6H); *m/z* (FABMS) 1496.7 [(M + Na)⁺, calc. 1496.6]. Found: C, 64.2; H, 6.5; N, 3.7; S, 4.0. Calc. for: C₈₁H₉₂N₄S₂O₁₈S₂·2H₂O: C, 64.4; H, 6.4; N, 3.7; S, 4.25%.

General procedure for the preparation of the complexes

To a solution of 1.0 equiv. of the triacid ligand and 4.0 equiv. of Et₃N in methanol was added 1.3 equiv. of the lanthanide nitrate salt. The resulting solution was stirred for 2 h, after which the solvent was concentrated to dryness. The complex was redissolved in ethyl acetate and washed twice with water to remove the excess lanthanide salt, followed by standard workup. The complexes were obtained as solids in nearly quantitative yields. The complexes all gave similar IR spectra: a peak at 1630 cm⁻¹ (ν_{NC=O}) with a shoulder around 1600 cm⁻¹. FABMS data: (Nd)**1**: *m/z* 1257.4 [(M + H)⁺, calc. 1257.4]; (Nd)**1a**: *m/z* 1386.7 [(M + H)⁺, calc. 1386.4]; (Nd)**2**: *m/z* 1267.4 [(M + H)⁺, calc. 1267.4]; (Nd)**2a**: *m/z* 1406.3 [(M + H)⁺, calc. 1406.5]; (Nd)**3**: *m/z* 1565.8 [(M)⁺, calc. 1565.5]; (Nd)**4**: *m/z* 1612.5 [(M)⁺, calc. 1612.5].

Photophysical studies

Steady-state luminescence measurements in the visible region were performed with a Photon Technology International (PTI) Alphascan spectrofluorimeter. The samples were excited with a 75 W quartz–tungsten–halogen lamp followed by a SPEX 1680 double monochromator. The emitted light was detected at an angle of 90° by a Hamamatsu R928 photomultiplier, and subsequently fed to a photon-counting interface. For steady-state measurements in the NIR region, the excitation light beam was modulated with a mechanical chopper at 40 Hz. The luminescence signal was detected with a liquid-nitrogen-cooled Ge detector, using standard lock-in techniques. Time-resolved luminescence measurements in the visible region were performed with an Edinburgh Analytical Instruments FL900 system. The excitation source consisted of a pulsed H₂-lamp (ns-pulsed output). The luminescence signal was detected by a Hamamatsu R928 photomultiplier and fed to a time-to-amplitude converter and a multichannel analyzer (Time Correlated Single Photon Detection). Luminescence lifetime measurements in the NIR region (Edinburgh Analytical Instruments LP900 system) were performed by monitoring the luminescence decay after excitation with a 0.5 ns pulse of an LTB MSG 400 nitrogen laser (λ_{exc} = 337 nm, pulse energy 20 μJ, 10 Hz repetition rate). Decay signals were recorded using a liquid-nitrogen-cooled Ge detector with a time resolution of 0.3 μs. The signals were averaged using a digitizing Tektronix oscilloscope. All decay curves were analyzed by deconvolution of the measured detector response and could be fitted with mono-exponential curves. The detector response was obtained by recording the signal of the NIR fluorescent dye IR 140 in methanol, which has a fluorescence lifetime (less than 1 ns) that is much shorter than the detector response.



Scheme 1 Reagents and conditions: *i*) dansyl chloride, Et₃N, CH₂Cl₂, rt; or 7-diethylaminocoumarin-3-acetic acid, EDC, DMAP, CH₂Cl₂, rt; *ii*) appropriate sulfonyl chloride, Et₃N, CH₂Cl₂, rt; or 7-dimethylaminocoumarin-3-acetic acid, EDC, DMAP, CH₂Cl₂, rt; *iii*) TFA.

Molecular mechanics (MM) and molecular modeling (MD) calculations

Initial structures as well as visualizations were carried out with Quanta 97.¹⁷ The MM and MD calculations were run with CHARMM 24.¹⁸ Parameters were taken from Quanta 97 and point charges were assigned with the charge template option in Quanta. The phenoxy oxygen atoms were charged to $-0.45e$. The ligand was charged to -3 , with a small "excess" charge smoothed to non-polar carbons and hydrogens. The parameters for Nd³⁺ were $\epsilon = 0.054 \text{ kcal mol}^{-1}$ and $\sigma = 3.47 \text{ \AA}$.¹⁹ The structures were minimized in the gas phase and then placed in a rectangular box ($31.49 \times 31.49 \times 47.23 \text{ \AA}$), initially filled with 400 OPLS DMSOs (OPLS = optimized potential for liquid simulations).²⁰ The protocol for molecular mechanics and dynamics has been described by van Veggel and Reinhoudt.²¹

Results and discussion

Synthesis

The synthesis of the dye-functionalized triacid ligands was carried out according to Scheme 1. The ligands were synthesized starting from the bis(amine) terphenyl **5** or mono(amide) terphenyl **6**, respectively.

Dansyl chloride was reacted with **6** or **5** to give the mono(dansyl) triester **7** and bis(dansyl) triester **7a** after flash column chromatography in 60% and 80% isolated yield, respectively. The ¹H NMR spectra of **7** and **7a** show four doublets and one multiplet in the region from 8.6 to 7.1 ppm for the protons of the dansyl moiety with a correct integral ratio compared to the signals of the benzylic protons (4H) of the terphenyl moiety. The coumarine triesters **8** and **8a** were synthesized by a DMAP (4-dimethylaminopyridine) catalyzed EDC [1-(3-dimethylaminopropyl)-3-ethylcarbodiimide] coupling of 7-(dimethylamino)coumarin-3-acetic acid and **6** or **5**, respectively, in CH₂Cl₂. The coumarine triester **8** was isolated after preparative thin layer chromatography in 52% yield and the bis(coumarine) triester **8a** was isolated after flash column chromatography in 48% yield. Formation of the amide bond was evident from the

¹H NMR spectra of these compounds. The ¹H NMR spectrum of the mono-functionalized compound **8** shows additional multiplet signals in the region around 5 ppm (compared to the ¹H NMR spectrum of **6**) corresponding to two benzylic protons of the newly formed amide moiety. In the ¹H NMR spectrum of the bis-functionalized compound **8a** multiplet signals around 5 ppm are present corresponding to four benzylic protons of the two amide moieties.

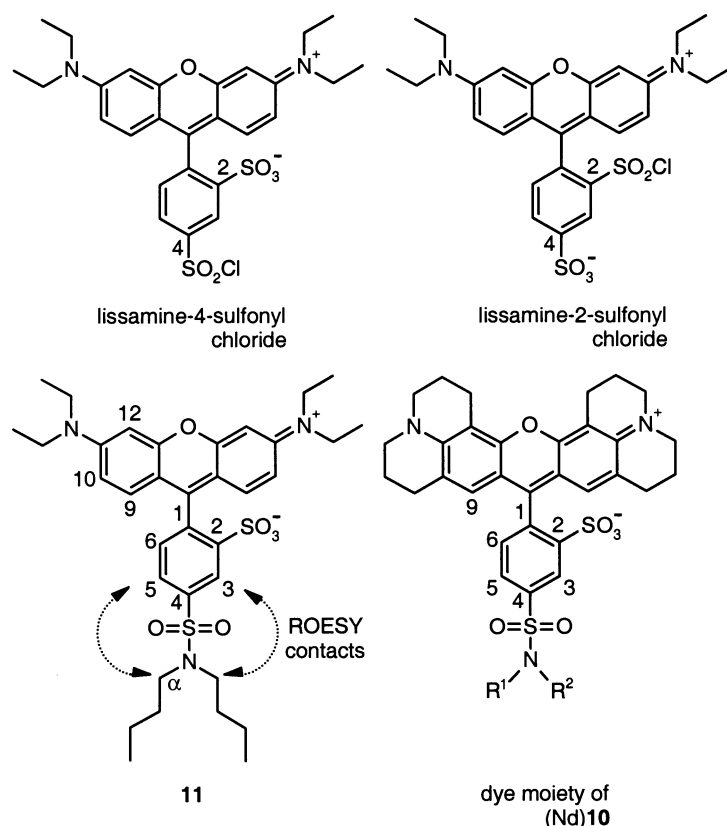
The terphenyl triester ligands functionalized with the Rhodamine-B derivatives lissamine and Texas Red were synthesized by reacting mono(amide) terphenyl **6** with the commercially available sulfonyl chloride isomer mixtures of the appropriate dye (Fig. 2).

Compound **11** was synthesized as a reference compound from di-*n*-butylamine and the lissamine isomer mixture (see Fig. 2) in CH₂Cl₂ in the presence of Et₃N as a base. One of the possible isomers (the 4- or the 2-isomer) of **11** was isolated after preparative thin layer chromatography in 40% yield. The ¹H NMR spectrum of the isolated product **11** shows one set of signals for the lissamine moiety (see Table 1), indicating that it is one compound and not a mixture of isomers. The assignment of the peaks was verified by a 2D-COSY²² experiment. The 2D-ROESY²³ spectrum of **11** shows contacts between the α -protons of the di-*n*-butyl tail and the H3 and H5 protons of the lissamine moiety (see Fig. 2), proving that the isolated product **11** is the 4-isomer.

Mono(amide) **6** was reacted with 2 equivalents of the lissamine isomer mixture, and only one of the two possible isomers (the 2-isomer or the 4-isomer) of lissamine triester **9** was isolated in 44% yield. The coupling of the dye was confirmed by mass spectrometry (FABMS): the spectrum shows an intense peak at 1615.8 that is attributed to $(M + H)^+$. The ¹H NMR spectrum of triester **9** shows one set of signals for the protons of the lissamine moiety (see Table 1) that is nearly identical to that of dibutyl lissamine **11**, indicating that the sulfonamide moiety of triester **9** is at the same position of the lissamine phenyl ring as the sulfonamide moiety of **11**. For the synthesis of the Texas Red triester **10**, mono(amide) terphenyl **6** was reacted with 2 equivalents of the Texas Red sulfonyl chloride

Table 1 Selected ^1H NMR data (300 MHz) of the compounds **9**, **10** and **11** in CDCl_3 . For numbering of the protons see Fig. 2

Compound	H3	H5	H10	H12
9	8.85 (s)	8.00 (d, $J = 8.5$ Hz)	6.81 (d, $J = 8.5$ Hz)	6.69 (s)
10	8.81 (s)	7.90 (d, $J = 7.8$ Hz)	n.a.	n.a.
11	8.74 (s)	7.91 (d, $J = 8.0$ Hz)	6.77 (d, $J = 8.0$ Hz)	6.66 (s)

**Fig. 2** Chemical structures of the isomers lissamine-4-sulfonyl chloride, lissamine-2-sulfonyl chloride, the model compound dibutyl-lissamine **11**, and the Texas Red moiety of **10**. The observed 2D ROESY contacts of **11** have been indicated.

isomer mixture, resulting in an isolated yield of **10** of 46% after preparative thin layer chromatography. The ^1H NMR spectrum of triester **10** shows one set of signals for the protons of the Texas Red moiety (see Table 1), and the chemical shifts of the H3 and H5 protons are almost identical to the chemical shifts of the corresponding protons of lissamine triester **9** and dibutyl-lissamine **11**. This shows that the isolated Texas Red triester **10** is also the 4-isomer.

Mild hydrolysis of the *tert*-butyl esters of the compounds **7–10** with trifluoroacetic acid at room temperature gave the corresponding triacid ligands in nearly quantitative yields. The corresponding Nd^{3+} complexes were prepared at room temperature by addition of a solution of $\text{Nd}(\text{NO}_3)_3$ in methanol to a solution of the appropriate ligand in methanol in the presence of Et_3N as a base. Mass spectrometry (FAB) showed that the complexes had the expected 1:1 stoichiometry (see Experimental). The IR spectra of the complexes (except for (Nd)**1a**) show an intense peak around 1630 cm^{-1} corresponding to the amide carbonyl, with a shoulder around 1600 cm^{-1} , indicating that the carboxylic acids are deprotonated. The spectra of (Nd)**1**, (Nd)**1a**, (Nd)**3**, and (Nd)**4** further show peaks around 1330 and 1160 cm^{-1} corresponding to the sulfonamides.

Molecular dynamics

The distance between the antenna and the Nd^{3+} ion plays a crucial role in the sensitization process since both the external heavy atom effect and the energy transfer process are strongly dependent on the distance. We have used molecular dynamics

simulations of the complexes in a solvent box of OPLS DMSO to estimate this distance. In the case of the dansyl antenna of (Nd)**1** and the coumarin antenna of (Nd)**2** the chromophore is directly attached to a Nd^{3+} coordinating group, and the distance is approximately 5 \AA . The actual chromophore of lissamine and Texas Red is the fused three-ring system. The simulations of (Nd)**3** and (Nd)**4** show that the phenyl ring is almost perpendicular to the three-ring system and in fact merely acts as a spacer. Therefore, the antenna– Nd^{3+} distance in (Nd)**3** and (Nd)**4** is larger and is approximately 10 \AA .

Luminescence

The incorporated fluorescent dyes have broad and intense absorption bands ranging from the near-UV to the visible region of the electromagnetic spectrum, dansyl has an absorption maximum at 345 nm ($\epsilon = 4.2 \times 10^3\text{ M}^{-1}\text{ cm}^{-1}$), coumarine at 400 nm ($\epsilon = 2.2 \times 10^4\text{ M}^{-1}\text{ cm}^{-1}$), lissamine at 568 nm ($\epsilon = 8.8 \times 10^4\text{ M}^{-1}\text{ cm}^{-1}$), and Texas Red at 590 nm ($\epsilon = 8.5 \times 10^4\text{ M}^{-1}\text{ cm}^{-1}$). The absorption spectra of the mono- and bis-functionalized complexes are similar (not shown), but as expected the absorption coefficients of the latter complexes are twice as high, 8.5×10^3 and $4.4 \times 10^4\text{ M}^{-1}\text{ cm}^{-1}$, for (Nd)**1a** and (Nd)**2a**, respectively.

Upon excitation of the antenna chromophores of the Nd^{3+} complexes in $\text{DMSO-}d_6$, the characteristic emission bands of Nd^{3+} were observed at 880 , 1060 , and 1330 nm (see Fig. 3). The intense emission band at 1060 nm corresponds to the $^4\text{F}_{3/2} \rightarrow ^4\text{I}_{11/2}$ transition, and constitutes approximately 60% of the total

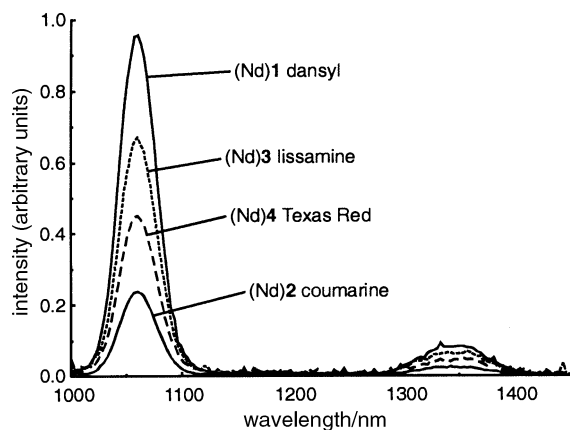


Fig. 3 Sensitized Nd^{3+} luminescence intensities of the dye-functionalized Nd^{3+} complexes in (Nd)1, (Nd)2, (Nd)3 and (Nd)4 in $\text{DMSO}-d_6$ upon excitation into the absorption maxima of the incorporated dyes. The luminescence spectra have been corrected for the absorbances of the samples and differences in the excitation intensity as a function of the excitation wavelength.

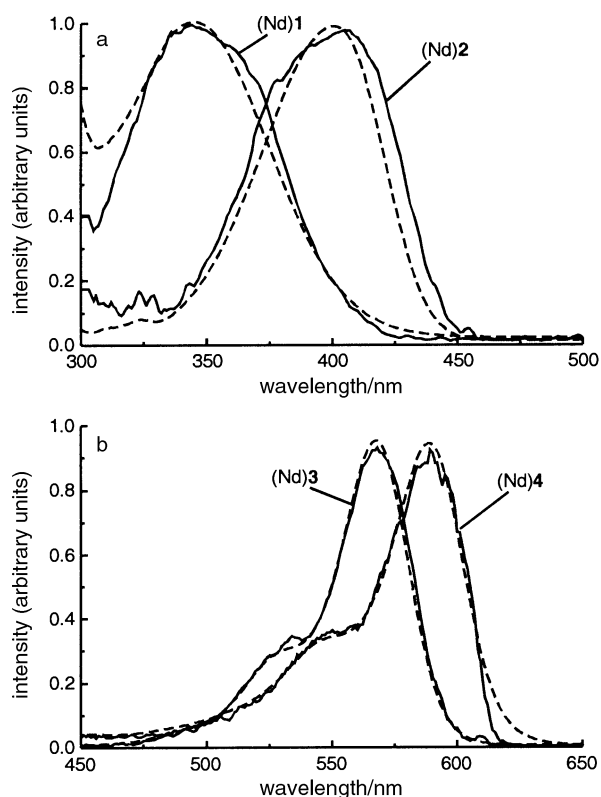


Fig. 4 Normalized excitation spectra (solid lines) of the dye-functionalized complexes (Nd)1 and (Nd)2 and (Nd)3 and (Nd)4 (b) in $\text{DMSO}-d_6$ while monitoring the intensity of the 1060 emission of Nd^{3+} , as well as the normalized absorption spectra of the dyes (dashed lines). The absorption and excitation spectra of (Nd)1a and (Nd)2a are identical to the spectra of their mono-functionalized derivatives.

emission intensity. The emission bands at 880 nm and at 1330 nm correspond to the ${}^4\text{F}_{3/2} \rightarrow {}^4\text{I}_{9/2}$ and ${}^4\text{F}_{3/2} \rightarrow {}^4\text{I}_{13/2}$ transitions, respectively.

The excitation spectra of the dye-functionalized Nd^{3+} complexes prove that excitation of the antenna is the main photo-physical pathway leading to Nd^{3+} luminescence. These spectra were recorded by monitoring the intensity of the 1060 nm emission band as a function of the excitation wavelength. As is clearly visible in Fig. 4, the excitation spectra closely resemble the absorption spectra of the incorporated antenna chromophores.

To enable a direct comparison of the sensitizing efficiency

Table 2 Sensitized emission intensity relative to the emission of (Nd)1 and luminescence lifetimes of the six different dye-functionalized complexes in $\text{DMSO}-d_6$

Complex	λ_{exc}	I_{SE}^a	$\tau_{\text{Nd}^{3+}}/\mu\text{s}^b$
(Nd)1	350 nm	1.0	2.21
(Nd)1a	350 nm	0.95	2.15
(Nd)2	400 nm	0.29	2.16
(Nd)2a	400 nm	0.26	2.39
(Nd)3	570 nm	0.75	2.21
(Nd)4	590 nm	0.53	2.26

^a Sensitized emission intensities of the 1060 and 1330 nm bands corrected for the absorbances of the samples and differences in the excitation intensity as a function of the wavelength and relative to (Nd)1. ^b λ_{exc} , 337 nm; λ_{em} , 1060 nm; error 10%.

of different dyes, the emission intensities in Fig. 3 have been corrected for the absorbances of the samples and differences in the excitation intensity as a function of the wavelength.²⁴ Under these conditions the emission intensities are proportional to the quantum yields of sensitized emission. In this series of fluorescent dyes dansyl is the most efficient sensitizer, followed by lissamine and Texas Red, and coumarine is the least efficient sensitizer (see also Table 3). The mono- and bis-functionalized complexes display similar sensitized emission intensities. The incorporation of an additional antenna chromophore does not increase the luminescence quantum yield of the system (*vide infra*).

In these experiments the solutions were not deoxygenated, and oxygen quenching could be an alternative pathway for the deactivation of the triplet excited state of the dye if the energy transfer rate has the same order of magnitude as the (diffusion-controlled) oxygen quenching rate, which is 10^7 s^{-1} .²⁵ The effect of deoxygenation of the samples on the sensitized luminescence intensity can therefore give an indication of the energy transfer rate. Whereas for most of the complexes no oxygen effect was observed upon deoxygenation of the samples, the luminescence intensities of (Nd)2 and (Nd)2a were oxygen dependent (an increase of 20% upon deoxygenation of the solvent). This indicates that the transfer of excitation energy from the coumarine antenna to the Nd^{3+} ion is slower ($k_{\text{ET}} \sim 10^7 \text{ s}^{-1}$) than for the other antenna chromophores ($k_{\text{ET}} > 10^7 \text{ s}^{-1}$).

The steady-state luminescence spectra depicted in Fig. 3 were taken for dilute solutions of the complexes (10^{-5} – 10^{-6} M), and demonstrate the effectiveness of using energy transfer for the population of the Nd^{3+} luminescent state. Direct excitation of the complexed Nd^{3+} ions would require concentrations of the samples of up to 0.1 M in order to observe any Nd^{3+} luminescence in solution^{26,27} as a result of the low absorption coefficients of the intra-4f transitions which are typically less than $10 \text{ M}^{-1} \text{ cm}^{-1}$.⁶ Furthermore, these low concentrations avoid the possible aggregation of the complexes since especially Rhodamine-B dyes tend to form dimers at higher concentrations.²⁸ The absence of such aggregation under the experimental conditions was confirmed by the fact that the sensitized Nd^{3+} emission intensity of the (Nd)3 and (Nd)4 complexes increased linearly with increasing absorbance of the samples up to an absorbance of 0.6 at the excitation wavelength.

The luminescence lifetimes of the Nd^{3+} -complexes in $\text{DMSO}-d_6$ upon laser excitation at 337 nm are equal within the experimental error: around 2.20 μs (see Table 2). These luminescence lifetimes are in line with the lifetimes of the *m*-terphenyl-based Nd^{3+} complexes,^{4,5} and the recently reported lifetime of $\text{Nd}(\text{OAc})_3$ of 2.33 μs in $\text{DMSO}-d_6$.²⁶ The energy gap between the lowest excited state (${}^4\text{F}_{3/2}$) and the highest ground state (${}^4\text{I}_{7/2}$) of Nd^{3+} is relatively small ($\Delta E \approx 5300 \text{ cm}^{-1}$), and non-radiative deactivation of the Nd^{3+} excited state by the first overtone of the C–H vibration, which has vibrational quanta of 2950 cm^{-1} , is therefore very efficient.

Table 3 Fluorescence intensities and lifetimes of the dyes in the complexes relative to fluorescence intensities of the dyes in the free ligands, as well as the estimated intersystem crossing rates using eqn. (1)

Complex	I/I_0	$\tau_{\text{complex}}/\text{ns}$	$\tau_{\text{ligand}}/\text{ns}$	$k_{\text{ISC}}/\text{s}^{-1}$
(Nd)1	0.14	2.88	16.8	2.9×10^8
(Nd)1a	0.30	2.37 (53%) 13.5 (47%)	16.9	3.6×10^8 (53%), 7.4×10^7 (47%)
(Nd)2	0.60	1.10	1.37	1.8×10^8
(Nd)2a	0.58	0.88	1.26	3.4×10^8
(Nd)3	0.30	1.22	2.60	4.4×10^8
(Nd)4	0.40	2.50	4.27	1.7×10^8

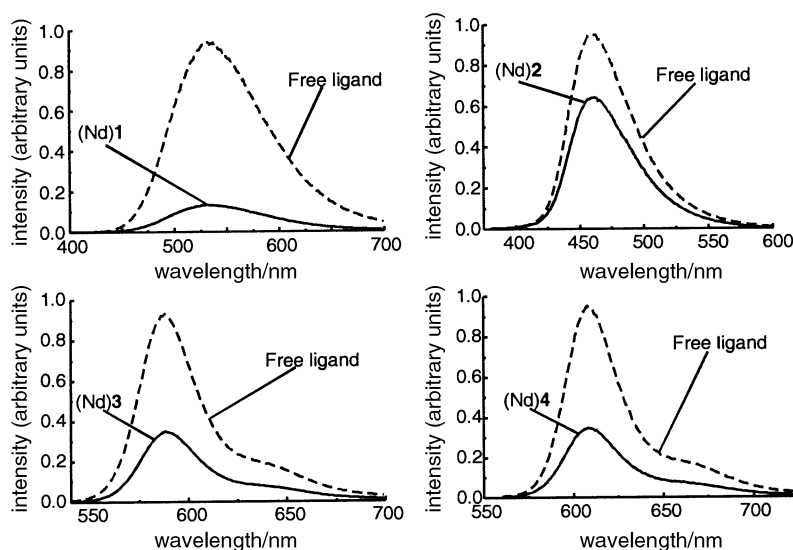


Fig. 5 The fluorescence intensities of the dyes in (Nd)1, (Nd)2, (Nd)3 and (Nd)4 relative to the fluorescence intensities of the dyes in the free ligands in DMSO. The dyes have been excited to their absorption maximum (see main text).

Antenna fluorescence

The antenna processes that are competing with intersystem crossing from the singlet state to the triplet state, are fluorescence and non-radiative decay (see Fig. 1). In the absence of the lanthanide ion, the dansyl, coumarine, lissamine, and Texas Red dyes have high fluorescence quantum yields, and as a result very low intersystem crossing yields (ϕ_{ISC} is typically less than 0.02).²⁹

The shape and the emission maxima of the fluorescence spectra of the dyes in the complexes and in the free ligands are similar, indicating that the complexed Nd^{3+} ion does not significantly affect the energy of the antenna singlet state (see Fig. 5). Especially in the case of the dansyl and coumarine antennas, it is somewhat surprising that coordination of the sulfonamide and the amide, respectively, to the triply charged lanthanide ions does not influence the singlet excited state. Fig. 5 clearly shows that the presence of the Nd^{3+} ion leads to a significant reduction of the antenna fluorescence intensity of the complex compared to the antenna fluorescence intensity of the free ligand. The reduction is the largest for the dansyl antenna of (Nd)1, which is more than 80%. The lissamine and Texas Red antennas of (Nd)3 and (Nd)4, respectively, display a similar decrease of the fluorescence intensity (more than 60%), whereas the coumarine antenna of (Nd)2 has the smallest reduction (40%) in the fluorescence intensity. The reduction of the fluorescence intensity of the dye in the complex is most probably caused by an external heavy atom effect induced by the presence of the heavy and paramagnetic Nd^{3+} ion. Due to spin-orbit coupling and paramagnetic interactions, the spin-forbidden singlet-triplet intersystem crossing process is enhanced,^{15,16} and this results in a reduction of the fluorescence intensity. The alternative processes that may deactivate the antenna singlet excited state in the presence of the lanthanide ion are singlet energy transfer and photo-induced electron transfer, but they can be ruled out. Singlet energy transfer to Nd^{3+} via a Förster

mechanism³⁰ is negligible because of the low oscillator strength of the 4f transitions of lanthanide ions. Also singlet energy transfer via an exchange mechanism³¹ is negligible because the radially contracted 4f orbitals lead to a small electronic matrix element for electronic exchange resulting in slow energy transfer rates with regard to the lifetime of singlet excited state.³² Photon-induced electron transfer is not possible, because unlike Eu^{3+} and Yb^{3+} , Nd^{3+} is not easily reduced.³³

The fluorescence lifetimes of the antenna moieties in the (mono-functionalized) complexes and free ligands are mono-exponential with lifetimes in the nanosecond region (see Table 3). The decreased lifetimes of the dyes in the complexes are in line with the observed reduction of the fluorescence intensities. The enhanced intersystem crossing rates can be estimated via eqn. (1).³⁴

$$k_{\text{ISC}} = 1/\tau_{\text{complex}} - 1/\tau_{\text{ligand}} \quad (1)$$

The results have been added to Table 3. The enhanced intersystem crossing rates of the four dyes in the complexes have the same order of magnitude, approximately 10^8 s^{-1} . Whether the enhancement in the intersystem crossing rate (k_{ISC}) also results in a large increase of the intersystem crossing quantum yield (ϕ_{ISC}) depends on the rates of the competing radiative (k_{rad}) and non-radiative (k_{nonrad}) decay of the antenna singlet excited state, see eqn. (2).

$$\phi_{\text{ISC}} = k_{\text{ISC}}/(k_{\text{ISC}} + k_{\text{rad}} + k_{\text{nonrad}}) \quad (2)$$

The dansyl antenna exhibits the largest increase in the intersystem crossing quantum yield, and thus the largest decrease in the antenna fluorescence intensity, mainly because of its relatively long-lived singlet excited state (16.7 ns). The singlet excited state lifetime of the coumarine antenna is much shorter (1.28 ns), and as a result, the overall effect is smaller.

The two antenna chromophores in (Nd)**1a** and (Nd)**2a** may influence their positions relative to the Nd³⁺ ion due to steric hindrance, or may interact by energy transfer from one antenna to the other. For the coumarine antenna chromophores of (Nd)**2a**, this is evidently not the case since the antenna fluorescence lifetimes and emission intensities of (Nd)**2** and (Nd)**2a** are comparable, as are the lifetimes and emission intensities of the corresponding free ligands. The bi-exponential fluorescence lifetimes of (Nd)**1a** suggest that there is an interaction between the two dansyl antenna chromophores, or more likely that one dansyl antenna is closer to the Nd³⁺ ion than the other. The dansyl antenna closest to the ion experiences the largest heavy atom effect and has therefore the shortest fluorescence lifetime. The dansyl antenna that is further away has less interaction and has a much smaller reduction in the fluorescence lifetime (compared to that of the free ligand). Since the fluorescence lifetime of the dansyl moieties in the free ligand is mono-exponential, this interaction does not take place in the free ligand. Since both antenna chromophores are probably capable of donating their triplet energies to the Nd³⁺ ion, this interaction does not strongly influence the overall sensitization process compared to the mono-functionalized dansyl complex (*vide supra*).

Discussion

As can be seen in Fig. 1, the sensitization pathway proceeds *via* the excitation of the singlet excited state, followed by the generation of the triplet excited state *via* intersystem crossing, and the subsequent energy transfer to the lanthanide ion. The overall quantum yield of sensitized emission is therefore the product of the intersystem crossing quantum yield, the energy transfer quantum yield and the luminescence quantum yield of the lanthanide ion [eqn. (3)].

$$\varphi_{\text{SE}} = \varphi_{\text{ISC}} \times \varphi_{\text{ET}} \times \varphi_{\text{lum}} \quad (3)$$

Since the luminescence lifetimes of the different dye-functionalized complexes are similar, the differences in the sensitized emission intensities (that are proportional to φ_{SE}) for the different complexes are due to the product of φ_{ISC} and φ_{ET} .

Due to relatively long-lived singlet excited state, the dansyl antenna has the highest induced φ_{ISC} . Moreover, the energy transfer to Nd³⁺ is independent of the oxygen concentration. As a result, the dansyl antenna is the most efficient sensitizer for Nd³⁺ luminescence. Despite the relatively large distance between the antenna and Nd³⁺ in (Nd)**3** and (Nd)**4**, there is an appreciable external heavy atom effect with intersystem crossing rates that are comparable to the dansyl antenna that is much closer to the Nd³⁺ ion. Also the energy transfer process is independent of the oxygen concentration. This shows that in addition to the distance, other factors such as structural differences of the dyes also play an important role. Compared to the dansyl antenna the induced φ_{ISC} of lissamine and Texas Red is smaller due to their shorter-lived singlet excited states. The coumarine antenna with the smallest induced φ_{ISC} and the oxygen dependent energy transfer is the least efficient sensitizer for Nd³⁺.

The incorporation of the additional antenna chromophore doubles the probability of the absorption of a photon compared to the mono-functionalized complexes. Under the experimental conditions, *i.e.* using a Xe lamp as the excitation source and dilute solutions, it is not likely that both antenna chromophores of (Nd)**1a** and (Nd)**2a** will be excited simultaneously. We have observed that the mono- and bis-functionalized complexes exhibited comparable sensitized emission intensities. One should bear in mind that the spectra have been corrected for the absorbance of the samples, and it shows that the incorporation of the second antenna chromophore does not affect the quantum yield of sensitized emission, but that it

increases the luminescence efficiencies ($\varepsilon \times \varphi_{\text{SE}}$) by a factor of two.

Conclusions

Despite their low intersystem crossing quantum yields, fluorescent dyes can be used as efficient sensitizers for near-infrared Nd³⁺ emission due to the increased intersystem crossing yield induced by the Nd³⁺ ion (the external heavy atom effect). Intramolecular energy transfer from the organic dyes dansyl, coumarine, lissamine, and Texas Red to Nd³⁺ has been established in the corresponding four *m*-terphenyl-based dye-functionalized Nd³⁺ complexes. The sensitization process is the most efficient in the dansyl complex (Nd)**1**, followed by the lissamine (Nd)**3** and Texas Red (Nd)**4** complexes, and least efficient in the coumarine complex (Nd)**2**. The complexed lanthanide ion was found to enhance the intersystem crossing rate of the antenna *via* an external heavy atom effect, as could be concluded from the reduced fluorescence intensities and lifetimes of the antenna in the complexes compared to the fluorescence intensities and lifetimes of the antenna in the free ligands. For the dansyl antenna, this results in a high intersystem crossing yield because of its relatively long-lived singlet excited state. The incorporation of an additional dansyl antenna increases the absorption coefficient of the resulting complex and also the luminescence efficiency ($\varepsilon \times \varphi_{\text{SE}}$) of the system. A drawback is that the excitation window is limited to 400 nm. For future applications, the lissamine antenna is the most attractive sensitizer, because it allows excitation at 530 nm, and its absorption coefficient is much higher.

Acknowledgements

Martijn Werts (University of Amsterdam) is gratefully acknowledged for his contribution to time-resolved antenna luminescence measurements. Akzo Nobel Research is gratefully acknowledged for financial and technical support. This research has been financially supported by the Council for Chemical Sciences of the Netherlands Organization for Scientific Research (CW-NWO).

Notes and references

- 1 E. Desurvire, *Phys. Today*, 1994, **97**, 20.
- 2 S. Ando, T. Matsuura and S. Sasaki, *CHEMTECH*, 1994, 20.
- 3 (a) B. Booth, *Polymers for Lightwave and Integrated Optics*, Ed. L. A. Hornack, Dekker, New York, 1992; (b) G. Karve, B. Bihari and R. T. Chen, *Appl. Phys. Lett.*, 2000, **77**, 1253; (c) D. An, Z. Yue and R. T. Chen, *Appl. Phys. Lett.*, 1998, **72**, 2806; (d) Q. J. Zhang, P. Wang, X. F. Sun, P. Dai, B. Yang, M. Hai and J. P. Xie, *Appl. Phys. Lett.*, 1998, **72**, 407; (e) M. H. V. Werts, J. W. Verhoeven and J. W. Hofstraat, *Appl. Phys. Lett.*, 1999, **74**, 3576; (f) Q. J. Zhang, P. Wang, X. F. Sun, Y. Zhai, P. Dai, B. Yang, M. Hai and J. P. Xie, *Appl. Phys. Lett.*, 1999, **74**, 3577; (g) S. Lin, R. J. Feuerstein and A. R. Mickelson, *J. Appl. Phys.*, 1996, **79**, 2868; (h) R. T. Chen, M. Lee, S. Natarajan, C. Lin, Z. Z. Ho and D. Robinson, *IEEE Photonics Technol. Lett.*, 1993, **5**, 1328; (i) C. Koeppen, S. Yamada, G. Jiang, A. F. Garito and L. P. Dalton, *J. Opt. Soc. Am. B*, 1997, **14**, 155.
- 4 S. I. Klink, G. A. Hebbink, L. Grave, F. G. A. Peters, F. C. J. M. van Veggel, D. N. Reinhoudt and J. W. Hofstraat, *Eur. J. Org. Chem.*, 2000, **10**, 1923.
- 5 S. I. Klink, L. Grave, D. N. Reinhoudt, F. C. J. M. van Veggel, M. H. V. Werts, F. A. J. Geurts and J. W. Hofstraat *J. Phys. Chem. A*, 2000, **104**, 5457.
- 6 K. A. Gschneider and L. R. Eyring, *Handbook on the Physics and Chemistry of Rare Earths*, North Holland Publishing Company, Amsterdam, 1979.
- 7 N. Sabbatini, M. Guardigli and J.-M. Lehn, *Coord. Chem. Rev.*, 1993, **123**, 201.
- 8 M. I. Gaiduk, V. V. Grigoryants, A. F. Mironov, V. D. Rmyantseva, V. I. Chissov and G. M. J. Sukhin, *J. Photochem. Photobiol., B*, 1990, **7**, 15.
- 9 S. B. Meshkova, N. V. Rusakova and D. V. Bolshoi, *Acta Chim. Hung.*, 1992, **129**, 317.

- 10 M. H. V. Werts, J. W. Hofstraat, F. A. J. Geurts and J. W. Verhoeven, *Chem. Phys. Lett.*, 1997, **276**, 196.
- 11 M. P. Oude Wolbers, F. C. J. M. van Veggel, F. G. A. Peters, E. S. E. van Beelen, J. W. Hofstraat, F. A. J. Geurts and D. N. Reinhoudt, *Chem. Eur. J.*, 1998, **4**, 772.
- 12 (a) S. Sato and M. Wada, *Bull. Chem. Soc. Jpn.*, 1970, **43**, 1955; (b) A. Haynes and H. G. Drickamer, *J. Chem. Phys.*, 1982, **76**, 114.
- 13 S. L. Murov, I. Carmichael and G. I. Hug, *Handbook of Photochemistry*, 2nd Edn., Marcel Dekker, New York, 1993.
- 14 M. H. V. Werts, J. W. Verhoeven and J. W. Hofstraat, *J. Chem. Soc., Perkin Trans. 2*, 2000, 433.
- 15 (a) S. Tobita, M. Arakawa and I. Tanaka, *J. Phys. Chem.*, 1984, **88**, 2697; (b) S. Tobita, M. Arakawa and I. Tanaka, *J. Phys. Chem.*, 1985, **89**, 5649.
- 16 W. Strek and M. Wierzchaczewski, *Chem. Phys.*, 1981, **58**, 185.
- 17 Quanta was bought from Molecular Simulations Inc., Burlington, MA, USA.
- 18 (a) B. R. Brooks, R. E. Brucoleri, B. D. Olafsen, D. J. States, S. Swaminathan and M. Karplus, *J. Comput. Chem.*, 1983, **4**, 187; (b) F. A. Momany, V. J. Klimkowski and L. Schäfer, *J. Comput. Chem.*, 1990, **11**, 654; (c) F. A. Momany, R. Rone, H. Kunz, R. F. Frey, S. Q. Newton and L. Schäfer, *J. Mol. Struct.*, 1993, **286**, 1.
- 19 F. C. J. M. van Veggel and D. N. Reinhoudt, *Chem. Eur. J.*, 1999, **5**, 90.
- 20 W. L. Jorgenson, BOSS Version 3.5 Biochemical and Organic Simulation System User's Manual, Department of Chemistry, Yale University, Connecticut, USA, 1994.
- 21 F. C. J. M. van Veggel and D. N. Reinhoudt, *Recl. Trav. Chim. Pays-Bas*, 1995, **114**, 387.
- 22 A. Bax and R. Freeman, *J. Magn. Reson.*, 1981, **44**, 542.
- 23 A. Bax and D. G. Davis, *J. Magn. Reson.*, 1985, **63**, 207.
- 24 Rhodamine-B was used as a quantum counter.
- 25 $k_{\text{quench}} = k_{\text{diff}}[\text{O}_2]$; k_{diff} is taken as $10^{10} \text{ M}^{-1} \text{ s}^{-1}$, $[\text{O}_2]$ in DMSO is 0.48 mM (ref. 13), therefore $k_{\text{quench}} = 0.48 \times 10^7 \text{ s}^{-1}$.
- 26 A. Beeby and S. Faulkner, *Chem. Phys. Lett.*, 1997, **266**, 116.
- 27 Y. Hasegawa, K. Murakoshi, Y. Wada, S. Yanagida, J.-H. Kim, N. Nakashima and T. Yamanaka, *Chem. Phys. Lett.*, 1996, **248**, 8.
- 28 (a) J. E. Selwyn and J. I. Steinfeld, *J. Phys. Chem.*, 1972, **76**, 762; (b) R. W. Chambers, T. Kajiwara and D. R. Kearns, *J. Phys. Chem.*, 1974, **78**, 380.
- 29 W. W. Mantulin and P.-S. Song, *J. Am. Chem. Soc.*, 1973, **95**, 5122.
- 30 T. Förster, *Discuss. Faraday Soc.*, 1959, **27**, 7.
- 31 D. L. Dexter, *J. Chem. Phys.*, 1953, **21**, 836.
- 32 G. Porter and M. R. Wright, *Discuss. Faraday Soc.*, 1959, **27**, 18.
- 33 The reduction potentials of Eu^{3+} and Yb^{3+} in water are -0.35 V and -1.05 V (vs. NHE), respectively. A. J. Bard, R. Parsons and J. Jordan, *Standard Potentials in Aqueous Solution*, Marcel Dekker Inc., New York, 1985.
- 34 Based on the low intersystem crossing yields of the antenna chromophores, it can be assumed that k_{ISC} is negligible in the free ligand thus $1/\tau_{\text{ligand}} = k_{\text{rad}} + k_{\text{nonrad}}$ and $1/\tau_{\text{complex}} = k_{\text{rad}} + k_{\text{nonrad}} + k_{\text{ISC}}$. It follows that $k_{\text{ISC}} = 1/\tau_{\text{complex}} - 1/\tau_{\text{ligand}}$.